Journal of Applied Fluid Mechanics, Vol. x, No. x, pp. x-x, 20xx.
Available online at www.jafmonline.net, ISSN 1735-3572, EISSN 1735-3645.
https://doi.org/10.47176/jafm.xx.xx.xxxxx

Design of F-16 Airfoil Mock-ups for Supersonic Wind Tunnel: Study, Production, Testing and Validation

N. Eddegdag[1†], A. Naamane[2], M. Radouani[1] and M. El Gadari[1]

[1] *Moulay Ismail University of Meknes, 15290, Meknes, Morocco*
[2] *Royal Air School, 40070, Marrakesh, Morocco*

†*n.eddegdag@edu.umi.ac.ma*

ABSTRACT

This research paper presents a comprehensive investigation into the behavior of viscous supersonic laminar flow and the Shock Wave- Laminar Boundary Layer Interaction (SWBLI) around the F-16 laminar NACA 6-series airfoil NACA 64A204. The study aims to establish and compare different methods for accurately describing these complex phenomena, which are of significant importance in the development of advanced aerospace technologies. To achieve this objective, a unique approach was adopted, involving the design and production of a mock-up F-16 airfoil equipped with pressure taps for use in the supersonic burst wind tunnel AF300. The mock-up was then experimentally tested, and the obtained data were analysed using numerical simulations with Ansys Fluent and a theoretical model based on a previously established analytical SWBLI model. The results obtained from the experimental, numerical, and analytical analyses validate the designed NACA 64A204 mock-up to a great extent. The study provides valuable insights into the physics of viscous supersonic laminar flow and SWBLI, contributing to a better understanding of these phenomena. The findings of this study will have important applications in the design of high-speed aircraft and other advanced aerospace technologies.

Keywords: Airfoil Mock-up; Laminar Viscous Supersonic Flow; Numerical Simulation; Experimental testing; SWBLI

NOMENCLATURE

NACA	National Advisory Committee for Aeronautics
SWBLI	Shock wave-boundary layer interaction
SBWT AF300	Supersonic burst wind tunnel AF300
SW	Shock wave
BL	Boundary layer
VDAS	Versatile data acquisition system
ABS	Acrylonitrile Butadiene Styrene
β	Ratio of maximum thickness and chord.
Re	Reynold number
φ	Velocity disturbance potential
δ	Similarity ration
C_{li}	Optimal lift coefficient
σ_{ext}	Experimental angle of the curved detached shock wave in extrados
σ_{int}	Experimental angle of the curved detached shock wave in intrados
ω_{ext}	Angle of Mach line in extrados
ω_{int}	Angle of Mach line in intrados
Δ	Distance between the curved detached shock and the leading edge
AOA	Angle of incidence
M_0	Mach number upstream of the airfoil
β_{ext}	Numerical angle of the curved detached shock wave in extrados
β_{int}	Numerical angle of the curved detached shock wave in intrados
μ	Mach angle
l_0	Boundary layer thickness
γ_{ext}	Angle of oblique shock wave at trailing edge
η	Normal coordinate in the Frenet coordinate system
$\bar{\eta}$	Non-dimensional normal coordinate in the Frenet coordinate system

m	Local incompressible Mach number linking the Lower Deck to the Main Deck
c	Airfoil chord
a	Mean-line designation, fraction of chord from the leading edge over which design load is uniform
y_c	Mean-line ordinate
$C_{li_{mod}}$	NACA 6A-series optimal lift coefficient
x	Distance along the chord
y	Distance perpendicular to the chord
y_t	Ordinate of symmetrical thickness distribution
t	Airfoil thickness ratio
ε	Airfoil parameter
$y(x)$	Wing airfoil equation
R	Radius of the leading edge
$y_c^{F16}(x)$	NACA64A204 mean-line ordinate
$y_t^{F16}(x)$	NACA64A204 Ordinate of symmetrical thickness distribution

1. INTRODUCTION

The understanding of the supersonic domain, a priori hostile, is crucial and essential from an operational point of view to master it and therefore ensure the achievement of various operational missions. It is also imperative in order to be able to respect the safety and integrity of aircrew and equipment.

The phenomena that appear due to the evolution of an aircraft in a supersonic flow, therefore, continue to be among the subjects of study and research, due to their complexity and lack of research in this particular field of study. One of the main key phenomena that govern and take place in supersonic flow are SWBLIs. In our previously published articles and studies, we tackled the modelling of laminar steady irrotational SWBLI around a thin airfoil located in the standard atmosphere. The modelling process initiated from Navier-Stokes equations adapted to our assumptions. We applied the asymptotic methods, adimensionnalisation and linearization, to obtain the equation governing our problem [1].

Following that, we respectively applied asymptotic expansions on these governing equations following physical parameters governing our case of study [β & Re^{-1}], and finally to obtain the formulas of perturbation velocity potential φ near the airfoil body far from the leading edge, both inside the boundary layer and in the undisturbed flow outside the boundary layer, we applied the singular perturbations methods in respect to the principle of least degeneracy.

The resolution process consisted of the adoption of the triple Deck Technic which divides the laminar boundary layer surrounding our obstacle [airfoil] into three major decks [Lower Deck, Main Deck and Upper Deck], in order to identify the constants in the formulas of perturbation velocity potential.[2]

The analytical model was validated numerically with Ansys Fluent and experimentally in the supersonic burst wind tunnel AF300 with a produced reduced airfoil NACA 5-series with pressure taps NACA 43013.[1]-[2]

However, the previous choice of airfoil wasn't ideal, since in our case study we started from the assumption of a laminar flow, which isn't accurate, especially when approaching the trailing edge of the chosen airfoil. Hence the results of the analytical-experimental-numerical comparison presented important differences and relative errors when approaching the trailing edge.

Thus, in this study we focus on a NACA 6-series laminar airfoil NACA 64A204, to perfectly describe the behavior of the flow around the airfoil and the different physical phenomena that take action in supersonic fields.

Hence, in the first part, we will tackle the different methods of design and production process of the F-16 airfoil mock-up with pressure taps in extrados for the Supersonic Burst Wind Tunnel AF300.

Secondly, we address the numerical approach in Ansys Fluent for the study of the problem under the same assumptions as in the analytical part [1].

Furthermore, the experimentation takes parts for the designed mock-up airfoil in the Supersonic Burst Wind Tunnel AF300, followed by an analysis and comparison of the experimental, numerical and analytical results for the NACA 64A204.

The aim of the experimental-analytical-numerical confrontation isn't only to validate our designed F-16 airfoil mock-up, but also to further refine our analytical model by detecting the different parameters that play a role in the behavior of the flow around supersonic laminar airfoils, that weren't addressed in the previous studies.

In addition, we aim to open the doors for several other airfoil mock-ups to be designed and to ensure maximum usage of the supersonic wind tunnel in the field of scientific research in order to be able to study the phenomena which interest the aeronautical field, and not only in pedagogical education, given that the latter is only equipped with a dielectric airfoil mock-up.

2. DESIGN OF THE NACA 64A204 F-16 AIRFOIL MOCK-UP

In itself, designing a scale model is not an easy task. Its size cannot be determined randomly, because the interpretation of the phenomena generated must also be verified on the real-size model. To do so, the reduced model must respect the notions of similarities. Otherwise, the "scale effect" claims that phenomena appearing with the model do not necessarily occur with the object in full size, and even if they reproduce this raises the question of how to transpose the results. [3]

2.1 Similarities Between Models

The first of the similarities to follow is geometrical similarity. It is carried out only when the dimensions of the reduced and real models are linearly homologous according to the same ratio δ, called the "similarity ratio". The models are then geometrically similar. In addition, this ratio is the basis of the industrial design, since it concretely represents the scale and then makes it possible to transpose any point from one model to another.[4]
In this project, this similarity is respected, as all dimensions are in per cent of chord length. Thus, the similarity ratio δ is described by the ratio of the reduced model chord to the real model chord:

$$\delta = \frac{c_{mock-up}}{c_{real}} \quad (1)$$

With $c_{mock-up}$ is the chord for the designed airfoil mock-up and c_{real} is the chord for the real aircraft airfoil.

2.2 Definition of the F-16 NACA 64A204 Airfoil

The three-dimensional wing of an aircraft is established from its two-dimensional section, called the airfoil. There are different types of airfoil categories in aeronautics.

In this specific case, it is a NACA airfoil. These airfoils are found on the majority of aircraft. They are airfoil designs for aircraft wings developed by NACA. They thus describe the shape of the airfoil thanks to a series of figures, which represent parameters in the equations generating precisely the section of the wing.

For the F-16, this is in particular the NACA 64A204 airfoil (see Fig. 1), described by 5 numbers and a letter. This follows a specific convention. All of the following % dimensions are in % chord length c.

The explanation of the numbers and the letter of the NACA 64A204 airfoil is as follows [5]:

- 6: indicates the series, this airfoil belongs to the NACA series 6 airfoils, which corresponds to the supercritical airfoils, with double camber.
- 4: corresponds to the position of the zone of minimum pressure, i.e., the position of the zone of maximum thickness, in tens of per cent.
- A: reflects the fact that from approximately 85% to the trailing edge, the trajectory of the middle line retains a constant steering coefficient [6].
- 2: indicates the optimum lift coefficient Cl_i, in tenths of a per cent.
- 04: describe the maximum thickness t, in per cent.

So, in other words, this supercritical airfoil has an optimal lift coefficient Cl_i of 0.2 and a maximum thickness t of 4% to 40%.

Moreover, the belonging of a NACA airfoil to serie-6 means that its geometry is deduced from its pressure distribution established in the wind tunnel. The 6-Serie also maximizes laminar flow by reducing drag.

The advantage of such an airfoil is that it has a very thin relative thickness, which leads to a high critical Mach number. On the contrary, this same small thickness close to the trailing edge can also become a drawback from the point of view of the design of the structure and of its manufacturing.[7]

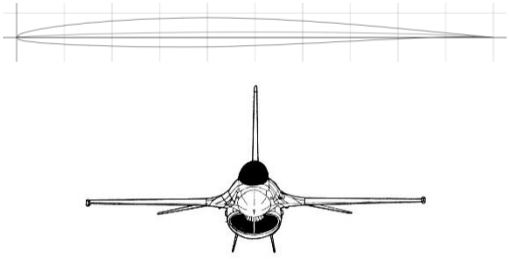

Fig. 1. F-16 NACA 64A204 Airfoil and F-16 schematics

2.3 Design of the F-16 airfoil Mock-up for the AF300 Wind Tunnel

The AF300 Rafale supersonic wind tunnel is equipped with a 100mm x 25mm dimension test section in which the 'scale' model of the airfoil is integrated.

2.3.1. Airfoil Modeling on CATIA V5

For this part, we introduce the airfoil parameters in the GNacaLt software (see Fig. 2). Then, we choose the maximum of points proposed, that is to say, 200. In order to be able to use this software correctly, the decimal symbol must be the point.

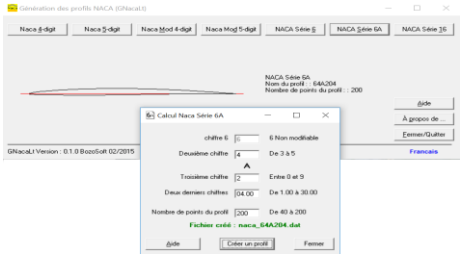

Fig. 2. GNacaLt Software

Secondly, we regroup these coordinates for extrados and intrados in per cent of the chord in a .dat extension file, which we transfer to the *GSD_PointSplineLoftFromExcel* spreadsheet in Microsoft Office Excel.
Furthermore, we transfer the Excel spreadsheet to CATIA V5 via the StarLoft option while activating Macros in the excel file, after interpreting the coordinates, CATIA attach the different uploaded points forming the airfoil (see Fig. 3).

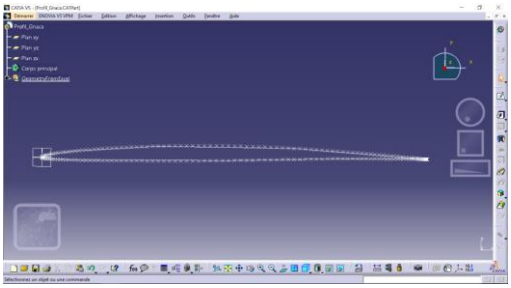

Fig. 3. NACA 64A204 Airfoil, Chord 60mm in CATIA V5 Software

Finally, we create a 3D mock-up of the NACA 64A204 with 60mm Chord, 25mm wingspan and two pressure taps in extrados with separate canalisation for air to enter and thus measure the exact experimental local pressure and Mach values in these pressure taps in the Supersonic wind tunnel AF300, in addition to that slots in the test stream of the wind tunnel AF300 to support the mock-up. (See Fig. 4) [8]

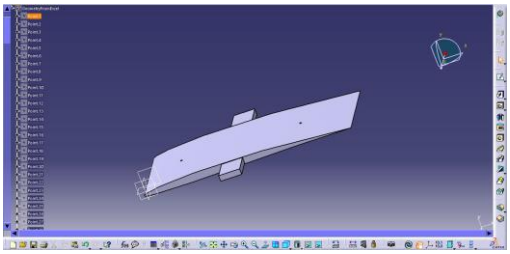

Fig. 4. NACA 64A204 Airfoil 3D Mock-up, Chord 60mm, width 25mm with two pressure taps with canalisation and mock-up supports for the slots, in CATIA V5 Software

2.3.2. Manufacturing of the NACA 64A204 Mock-up

For the manufacturing of the airfoil NACA 64A204 mock-up, two methods were proposed:

- 1st method: by 3D printing
- 2nd method: A mock-up of the airfoil by laminate bronze, followed by a canalization by pipes and filling with polyester putty

a. 3D Printing of the NACA 64A204 Mock-up

3D printing did not fully meet expectations. Indeed, as explained before, the design of airfoils with a very low relative thickness encounters difficulties in achieving the trailing edge. Here, the dimensions of the models are too thin for the 3D printer, which is therefore unable to finish the trailing edge from about 90-95% of the chord. Thus, all scale models are approximately 5 *mm* missing.

In addition, the models seemed fragile and had imperfections in their surface condition., and the pressure taps weren't doable due to the fragility of the used material and the small diameter of the pressure taps' canalization (see Fig. 5).

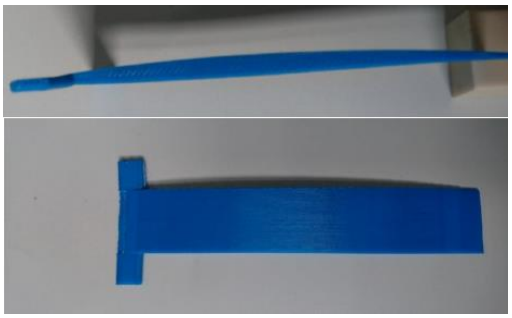

Fig. 5. NACA 64A204 Airfoil 3D printed mock-up with 100mm chord

b. Manually Manufactured NACA 64A204 Mock-up

Note that this method will allow us to have pressure taps on the extrados and the intrados (simultaneously). Thus, we can evaluate the variations of the Mach number along the airfoil (unlike the dihedral airfoils where we only need the pressure taps on the extrados given the symmetry of the airfoil).
Our model is made in three parts: the two sides of the airfoil and a closed box with a stressed coating (see Fig. 6). For the two static pressure taps on the extrados, a channel was designed using pipes with a radius of 1.5mm. Then, the airfoil mock-up is filled with polyester putty (material that resists high pressures and temperatures to prevent deformation and give weight to the mock-up). Finally, the assembly is soldered by a silver gun.

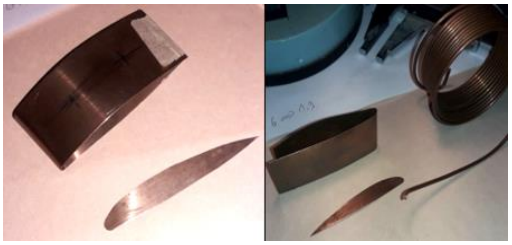

Fig. 6. Images of the surfaces and piping constituting the manufactured airfoil mock-up

Finally, it was possible to produce the airfoil mock-up NACA 64A204 (F-16) with two pressure taps on the extrados (see Fig. 7), with the following properties:

- Chord 100mm
- Maximum thickness = 100 x 4% = 4 mm
- Pressure taps at the leading edge at 30%$_c$ x_1=30mm
- Pressure taps at the trailing edge at 60%$_c$ x_2=60mm

Fig. 7. NACA 64A204 Airfoil mock-up with two pressure taps in the extrados and a 100mm chord

3. EXPERIMENTATION IN THE SUPERSONIC BURST WIND TUNNEL AF300

In the aeronautical field, wind tunnel testing remains an essential element. However, they are not trivial. Indeed, the AF300 wind tunnel has a particular operating regime, because it is a supersonic burst wind tunnel. On the other hand, it should be noted that the flow created by this machine is also subject to the scale effect and must therefore respect similarity conditions.

The complete similarity concerns the flows and adds dynamic similarity to the geometrical similarity. For the flow of the experiment and that under real conditions to be similar, they must respond to their balance equations in dimensionless form with an identical solution, thanks to initial conditions and limits of the same order. This is possible only when their dimensionless characteristic numbers, determined according to the principle of dimensional analysis, are equal.[8]

However, this last principle is in reality difficult to obtain. It is then necessary to concentrate on the characteristic number translating the phenomenon which plays the most important role, to validate a restricted similarity.
In particular for this study, concerning the flow of a compressible fluid like air, it is necessary to take into account the effects of compressibility in addition to the effects of viscosity. So, the characteristic numbers, in this case, correspond to the Mach number M and the Reynolds number Re.

3.1 Experimental Tests and Results

The AF300 supersonic wind tunnel is a Göttingen type return wind tunnel. More specifically, it is an economical scaled-down laboratory wind tunnel allowing experiments to be carried out at air speeds of Mach 1.4 and 1.8. It has three different parts: the wind tunnel duct, the test section and the instrumentation panel.

For our two conducted experimental studies, the operating conditions (see Table I) are presented as follows:

Table 1 Operating Conditions for NACA 64A204 In SBWT AF300

Time	**Operating conditions**		
Time	Liner	ATM Press	Model Angel AOA
[s]	---	[mbar]	[degree]
0.00	Mach 1.8	915	-1.1

3.1.1 Experiments for the 3D-printed mock-ups

The experiment aims to determine via VDAS the Mach number at a point on the upper surface and lower surface, thanks to the new pressure taps 26 and 27. It can then be compared with those established by theoretical and numerical models. In a second step, with the Schlieren device, the shock waves at the leading and trailing edges can be visualized, possibly with the expansion waves.

However, the fragility of the mock-ups, which are made of ABS, made the experiments complex. At the end of the experiment, all the mock-ups were destroyed in the SBWT AF300, because the hooks could not withstand the supersonic gusts, as shown in Fig 8.

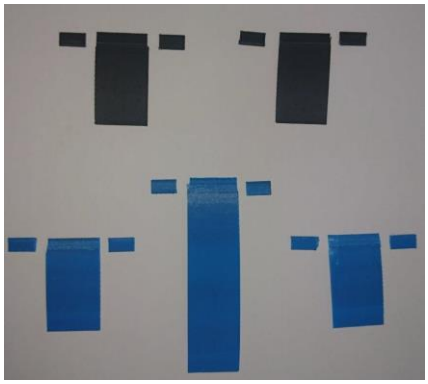

Fig. 8. Deteriorated 3D-printed NACA 64A204 mock-ups

The mock-up with a 30mm chord, reduced to 25mm after 3D printing, was the only one that held in place long enough to visualize, albeit faintly, the curved detached shock waves, below, the leading edge with the Mach 1.4 SBWT AF300 nozzle. (See Fig.9)

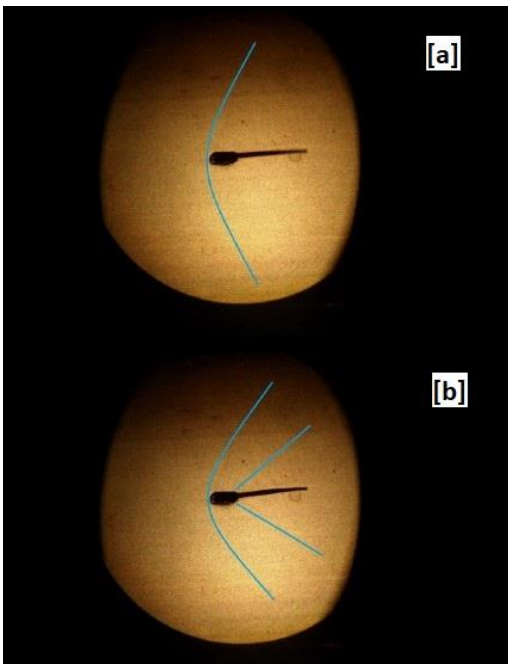

Fig. 9. Detached curved shock wave visualization for the 25mm chord's NACA 64A204 mock-up

Photo [a] was taken at the beginning of the experiment, the second half through. Thus, the shock on [b] is tighter on the walls because the speed of the flow has increased. Also likely, the mock-up is subjected to very virulent vibrations which make it move, this could in another way explain the fact that the shock waves are different between these two photos.

Photo [b] also shows two expansion waves visible on the extrados and the intrados. They seem to correspond to Mach lines and are also more stuck to the walls.

In the two photos, the oblique shock wave at the trailing edge is not visible, certainly because the vibrations were the most intense there.

By graphic measurements on the second photo, which is the most usable, the angles of the curved detached shock wave are: σ_{ext}=55° and σ_{int}=58°. Those of the expansion waves measure: ω_{ext}=34.5° and ω_{int}=36.5°. Then, the distance Δ between the curved detached shock and the leading edge is estimated to equal $\Delta = 0.87\ cm$.

The angles of the shocks on the lower surface should be lower than those on the upper surface because the angles of deflection are greater there. This may come from the approximation of the representation of the shock waves around the airfoil since the measured angles' data are unreliable but remain consistent with the order of magnitude.

These parameters are the only ones that could be evaluated during the various experiments of the project. They nevertheless transcribe experimental phenomena on which this project can be based. In particular, these empirical values will be used when compared to rational values.

3.2 Experiments for the manually manufactured mock-ups

After focusing on the smooth running of the experiments, we, therefore, began to extract several readings of values of local static pressure from the pressure taps in the extrados, with the Mach 1.8 nozzle airfoil, so we obtained the following results for the reduced wing airfoil NACA 64A204 (see Table 2):

Table 2 Recording of Local Mach Number Values in the Pressure Taps for NACA 64A204 from VDAS

Mach Upstream	Pressure Tap	Local Experimental Mach Number
1.55	Pressure Tap N^{26}	1.42
1.55	Pressure Tap N^{27}	1.47
1.44	Pressure Tap N^{26}	1.33
1.44	Pressure Tap N^{27}	1.38

Thus, we see that the Mach number in extrados increases from the 1st pressure tap to the 2nd due to a supersonic expansion fan. Through such an expansion [Prandtl–Meyer expansion fan], the flow remains isentropic, and our hypotheses then remain verified. There is a decrease in pressure and an acceleration of the fluid upstream.

4. Experimentation in the Supersonic Burst Wind Tunnel AF300

In this part, the numerical approach for the study will be presented, under the same assumptions as in the theoretical part [1]. Indeed, it will make it possible to obtain the precise behaviour of a viscous supersonic laminar airflow around the NACA 64A204 airfoil after setting the Ansys Fluent 2022 R2 simulation software parameters.[9]

4.1 Definition of Geometry

The geometry definition, by the ANSYS DesignModeler software, concerns two elements. We must first create the object, therefore our wing airfoil. Then, it is just as important to establish the calculation domain, including of course the airfoil.

4.1.1 The Airfoil

Regarding the object, it can be modelled using different methods. For example, the airfoil coordinates can be entered directly into ANSYS Fluent, then the software generates the surface itself. In this project, it was rather preferred to draw it with SOLIDWORKS software and then import it later into the digital simulation software, therefore, requires investment before actually using the software.

To do this, using the GNacaLt software, a freely downloadable airfoil generator, it was possible to recover a file (.txt) containing 200 exact coordinates of the NACA 64A204 airfoil. Then, the CAD software can interpret them in space and thus propose a geometry of the airfoil.

Once this preparatory work has been done, the digital simulation software can be launched.

In the interface assigned to geometry, ANSYS DesignModeler, the drawing under CATIA must be imported and generated, ensuring that it is represented in the correct plane.

4.1.2 The Study Domain

In this area, the calculations will be applied and the equations will be solved. It is concretely a viewing window through which the flow is studied.

In this study, after several dimensional tests, the calculation domain below (see Fig.10.) was selected because it dispenses with the airfoil of the phenomena mentioned just above.

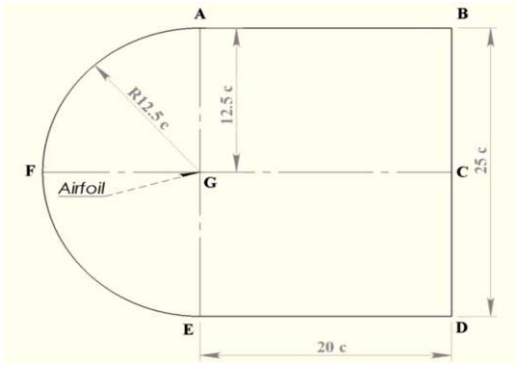

Fig. 10. Proposed Study Domaine for the airfoil

There are now two distinct surface-type objects saved in the software. But, in this state, it could not take into account the effects of the airfoil on the flow in the domain. It will then be necessary to merge these two surfaces, or rather subtract them. Indeed, it is necessary to create a new surface corresponding to that of the calculation domain above from which that of the airfoil must be removed. (See Fig.11.)

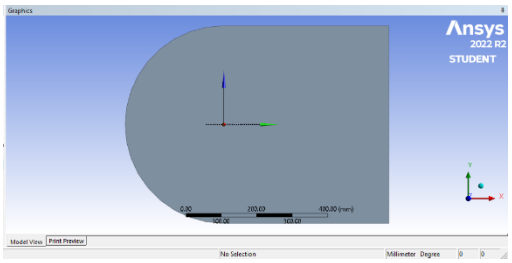

Fig. 11. Study Domain in Ansys Fluent 2022 R2 for Meshing

It must be considered that the airfoil is now fully integrated into the final calculation domain.[10]

Consequently, this last domain is the one that must be meshed, since the calculations taking place there take into account the presence of the airfoil in the flow.

4.2 Meshing

Under ANSYS Meshing, the Finite Element Method (FEM), used by ANSYS Fluent, requires a division of the final domain through a mesh. It is concretely about its spatial discretization. In other words, the entire domain is geometrically modelled by many smaller domains. The interest of meshing is to obtain the simplification of the simulations of calculations.[10]-[11]

The mesh quality has great importance on the results obtained by a numerical calculation. To do this, we first generate a coarse mesh (automatic) which we then improve by Face Sizing technic in meshing based on a Sphere Influence option to furthermore refine the mesh around the airfoil, followed by an All-Triangle Mesh Control Method, then we insert an Inflation Option to take into account the effect of the boundary layer, and last, we perform a Pinch Control to remove small features at the mesh level to generate better quality elements around those features. Finally, a second modification is to introduce a progressive refinement as the airfoil moves away.

Hence, we end up with a Meshing of 1,689,093 Elements and 847,438 Nodes. (See Fig.12.)

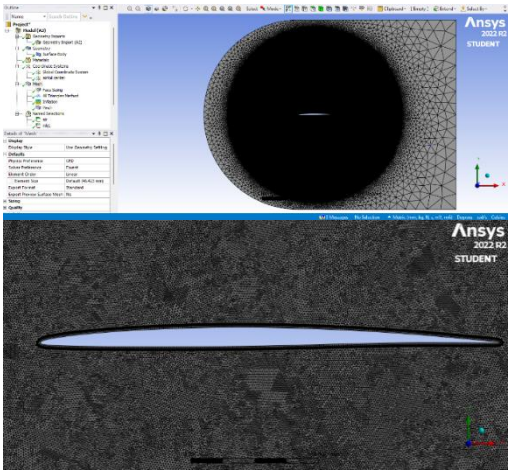

Fig. 12. Final Refined Mesh in Ansys Mesher 2022 R2

The numerical resolution procedure can therefore be initiated.

4.3 Calculation Process

4.3.1 Configuration Of Solver Settings

Before launching calculations, the following parameters must be configured:

- An adopted model (for our problem we will take the laminar viscous model with energy equation)
- Fluid parameters (air):
  - *Air density = 1.225 kg.m^{-3}*
  - *Air viscosity = 1.7894.10^{-5} kg. (m.s)$^{-1}$*
  - *Sound speed in air = 347.092 m. s^{-1}*

For the boundary conditions, it is possible to establish the conditions for the evolution of the flow on the walls of the domain, then on the extrados and the intrados.

On the four outer walls of the calculation domain, the initial conditions are established as if the domain were open to immerse the airfoil in it. It is necessary to specify the value M_0 of the Mach number upstream of the airfoil according to the direction of the flow [*for our case since in the experimental study we have an AOA=-1.1°, thus we have the flow in a direction of*

$$\overrightarrow{flow_{direction}} = cos(-1.1°)\,\vec{x} + sin(-1.1°)\,\vec{y} \quad (2)$$

, and to enter the atmospheric pressure, as well as the temperature. Moreover, in the case where the fluid is viscous, it is necessary to impose a condition of a "sliding wall" on the upper and lower walls of the domain to force the flow to remain straight there without friction. Then, for the extrados and the intrados, the solver must be informed that these are simple walls immersed in the flow.
Thus, once the parameters have been saved, we can start the calculation process.

4.3.2 Calculation Process

The solver starts from the initial solution and, thanks to an iterative algorithm for solving the matrix system obtained by discretization, it will perform iterations of the problem. Each iteration must modify the current solution and replace it with a solution closer to the exact solution sought. The solver gives at each iteration and for each equation the residual.

Moreover, during a simulation, it is interesting to focus on the convergence of the calculation residuals. Indeed, at each iteration and for each equation, an error, called "residual", is evaluated concerning an exact solution to the problem. And, it is said that a computation converges if the residuals decrease during the iterations. Thus, a result is only valid if the residuals converge (See Fig.13.). If the residuals do not converge sufficiently, the operation must be repeated until they converge properly.

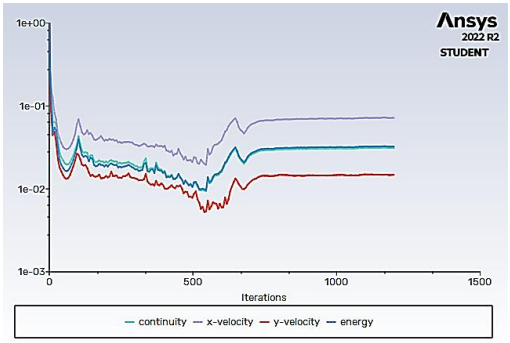

Fig. 13. Evolution of residuals according to iterations

4.4 Visualization And Analysis of Results

The numerical resolution will initially allow checking if the geometry and the mesh have been correctly parameterized thanks to the consistency of the results, and will allow a second time to visualize the behavior of the flow according to the solver settings. The simulation step is very important because it allows us to determine the domain of validity of our model.

4.4.1 NACA 64A204 for M_0=1.44

For M_0=1.44, with the parameterization established above and after convergence of the residuals, Figure 14 below is obtained. It represents the behavior of the flow through the evolution of the speed and the Mach number in the final computational domain. The different velocity values are displayed by colour. It also reveals three particular phenomena due to the presence of the airfoil in the supersonic flow.

First of all, it allows visualizing the variation of the velocity from the leading edge and all along the airfoil. In particular, it is observed that on the upper surface the velocity keeps increasing from the leading edge to the trailing edge where $M^{1.44}_{ExtradosTrailingEdge} = 1.5305$ .While on the lower surface, it grows faster from the leading edge up to 50% of the chord where $M^{1.44}_{Intrados50\%} = 1.5004$, then decreases to the trailing edge where $M^{1.44}_{IntradosTrailing\ Edge} = 1.4497$, which translates due to the double camber of the NACA64A204 airfoil.

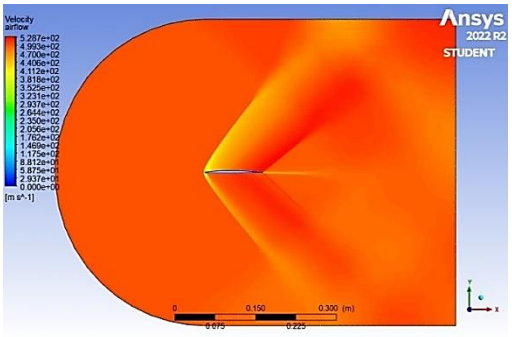

Fig. 14. Evolution of velocity along the NACA64A204 airfoil for M_0=1.44

Secondly, the figure 15 depicts the curved detached shock wave on the leading edge, with the presence of a blue-green sonic stagnation bubble, where M<1.00, where the flow is locally rotational subsonic incompressible and that is due to the curved quasi-hemispherical nature of the airfoil and the supersonic nature of the flow. As for the vicinity of the trailing edge, only the shock wave attached obliquely to the upper surface is visible. Finally, the expansion waves in form of Mach Lines appear clearly on the airfoil in form of a Prandtl-Meyer expansion wave that is due to the convex and concave forms of the airfoil curves along its extrados and intrados

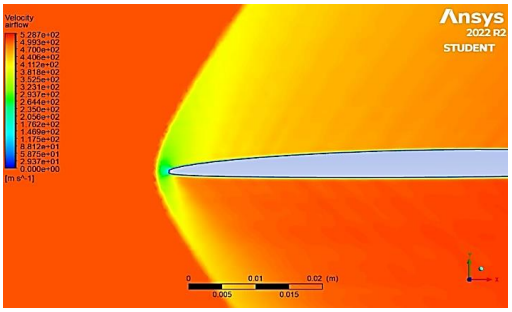

Fig. 15. Visualization of SW and Sonic Bubble for NACA64A204

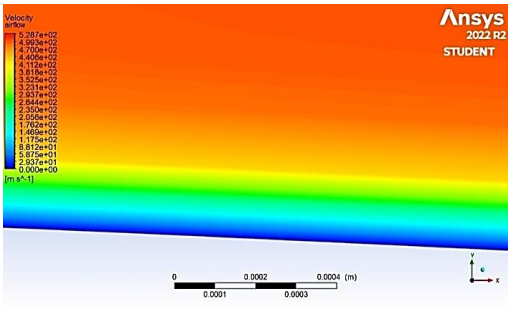

Fig. 16. Visualization of the Triple Deck Boundary Layer around the NACA 64A204 airfoil by Simulation on Ansys Fluent

Finally, by graphical measurements in Figure 15, the shock angles of the curved detached wave are worth at the leading edge: β_{ext}=62° and β_{int}=60°. These angles are between 90° and the Mach angle of $\mu=arcsin(1/M_0)$ = 43.983°. Similarly, the angle at the trailing edge is equal to γ_{ext}=40°.

The angles β_{ext} and β_{int} are not the same because the airfoil is not symmetrical. Thus, it happens $\beta_{ext}>\beta_{int}$ since the angle of deflection of the flow on the upper surface is greater than that on the lower surface.

On the other hand, the distance Δ_{num} between the curved shock wave and the leading edge is graphically worth: Δ_{num}=2.687 cm.

Finally, the third observed phenomenon is the shock wave-boundary layer interaction, which is the result of viscous supersonic flow. According to figure 16, we note the existence of a boundary layer all along the wall of the thickness airfoil l_0=0.3076mm where the Mach is subsonic and the speed tends towards a zero-value approaching the surface of the airfoil. Thus, the fluid particle (air) adheres to the wall (no-slip condition). It is also clear the three sub-layers of the boundary layer (viscous sub-layer in dark blue, main layer in sky blue and the upper layer in green) highlight our triple-deck model chosen during the theoretical part. We also note the existence of shock waves after the boundary layer (in height, Prandtl-Meyer expansion fan) where the Mach is supersonic, which highlights the phenomenon of the shock/boundary layer interaction. [12]

Thus, the local Mach number goes from a subsonic value in the boundary layer ($M<1$) to a supersonic value during shock waves where the external flow is supersonic ($M>1$), by a sonic line where the local Mach number along this line is equal to 1, to characterize and allow the subsonic-transonic-supersonic transition. [13]

For comparison, it is interesting to run the calculation again for a different upstream Mach number M_0.

4.4.2 NACA 64A204 for M₀=1.55

For $M_0=1.55$, with the same parameterization and still, after convergence of the residuals, results are obtained. The same phenomena of SWBLI and Curved Detached SW with the clear appearance of the triple-layered BL appear with increasing width of $l_0'=0.4262mm$.

Similarly, it is observed that on the upper surface the Mach number keeps increasing from the leading edge to the trailing edge where $M^{1.55}_{ExtradosTrailingEdge} = 1.606$ While on the intrados, it also grows faster from the leading edge to the same position at 50% of the chord where this time $M^{1.55}_{Intrados50\%} = 1.579$, to then decrease to the trailing edge where $M^{1.55}_{IntradosTrailingEdge} = 1.545$.

Additionally, the curved detached SW, here tighter on the leading edge, with the presence of a blue-green sonic bubble, where $M'<1.00$, with a larger radius. Then, near the trailing edge, the oblique attached shock wave is still only visible on the upper surface. Finally, the expansion waves always appear clearly on the profile.

In the same way as for the previous simulation, by graphic measurements, the shock angles of the curved wave are worth in this case: β'_{ext}=55° and β'_{int}=52°. These angles are, likewise, between 90° and $\mu'=arcsin(1/M_0)$ =40.1778°<μ, corresponding to the minimum shock angle. Moreover, that at the trailing edge is equal to γ_{ext}'=30°<γ_{ext}.

For the distance Δ_{num}', it finally comes graphically here: Δ_{num}'=1.124 cm<Δ_{num}.

Consequently, it is deduced that the higher the velocity of the upstream flow, the smaller the angle of the curved detached shock wave for the same profile, and the greater the distance between this shock is the edge of attack is small.

The first simulations are thus completed and analysed. However, it was expected to obtain a great finesse of the solutions according to the mesh and the

established settings. Now, from these figures, the results look coarse along the different shock waves, especially for a high M_0. We must therefore find a way to be even more precise in post-processing simulations.

4.4.3 From Simulation to Analytical Model Improvement

Based on our previous published studies concerning the modelling of the laminar SWBLI around a thin airfoil [1]. And, as a reflection and application of our soon-to-be-published study entitled '*Improved Analytical/Statistical Modelling of the Shock Wave-Laminar Boundary Layer Around a Thin Airfoil: Standard Atmosphere Case'* [2]. We tend similarly for our object of this study F-16 airfoil NACA64A204, to improve Analytically/Statistically the analytical model for the F-16 airfoil to obtain the most accurate analytical results for the confrontation and validation of our mock-up and exact description of the multitude of phenomena that govern the supersonic laminar viscous flow around F-16 laminar thin airfoil.

For the NACA 64A204 series-6 airfoil with coefficient β=0.04, the Local Mach numbers are compared on the upper surface and lower surface in the wall far from the leading edge, thus the position of the maximum relative camber characterizes the end of the zone from the leading edge. It is known for every NACA wing profile. Generally, it is defined by the second digit of the series, for the NACA 64A204 profile it is 4% of the chord, so we perform our calculations and extract our results for x greater than 0.04. In addition, we take different points in the 3 parts of the profile function as well as different altitudes of η (in the boundary layer and outside the boundary layer), to be able to check our model. Similarly, we have that $0 \leq \bar{\eta} \leq 0.13257143$, as well as *y* must be between 0 and 0.132 for *x* between 0.006158 and 1.

Thus, for $M_0=1.44$, we have that the equation for the Link Mach Number *m* (Local incompressible Mach number linking the Lower Deck to the Main Deck) is the following:

$$m^{1.44}_{NACA64A204}(\bar{\eta}, \bar{s}, M_\infty) = 21.0474\bar{\eta} - 2.5406\bar{s} - 0.0722 \quad (3)$$

Same for $M_0=1.55$, we have that the equation for the Link Mach Number is the following:

$$m^{1.55}_{NACA64A204}(\bar{\eta}, \bar{s}, M_\infty) = -35.6199\bar{\eta} + 2.8276\bar{s} + 0.7234 \quad (4)$$

5. Confrontation Of Analytical-Numerical-Experimental Results

The aim of this chapter is to compare our experimental results of the Local Mach numbers in Pressure Taps 1 and 2, to the results of the Local Mach numbers in the same coordinates from simulation in Ansys Fluent and the analytical results based on our improved analytical model [2]. The comparison will lead not only to the validation of the designed mock-up of the F-16 airfoil, but also to further elaborate the phenomena that take place in SWBLI around the F-16 wing.

5.1 Analytical results

Our analytical results for the Local Mach numbers for NACA64A204 airfoil in the extrados at 30% and 60% of the chord ($c=100mm$) are calculated from our previously established velocity formulas from our previous studies [1]-[2]. However, since these formulas are in the Frenet coordinate system, it is imperative to establish these formulas in the cartesian system by first and foremost establishing the NACA64A204 airfoil equation.

5.1.1 NACA 64A204 Wing Section Equation

The NACA airfoils are constructed by combining a thickness envelope with a camber or mean line. The 6-series mean lines were designed using Thin Airfoil Theory to produce a constant loading from the leading edge back to $x/c = a$, after which the loading decreases linearly to zero at the trailing edge. The term a, not to be confused with the speed of sound in air, denotes a particular position on the string. [14]

Indeed, the camber line of a Series-6 NACA airfoil produces a uniform loading along the chord from the leading edge at $x/c=0$ to the point $x/c=a$, then produces a linearly decreasing load from that point to the trailing edge at $x/c=1$. Generally, a is greater than or equal to the position of maximum thickness. For a series 6A-NACA airfoil, this parameter is approximately equal to: $a=0.8$. And for this particular airfoil, it is equal to: $a=0.831$.
The equation of the mean line for the 6-series NACA airfoil is the following [15], which is a simplification of the original expression for mean-lines ordinates given in [16]

$$\begin{cases} \frac{y_c}{c} = \frac{C_{li_{mod}}}{2\pi(a+1)\left\{\begin{matrix} \frac{1}{1-a}\left[\begin{matrix} \frac{1}{2}\left(a-\frac{x}{c}\right)^2 log_e\left|a-\frac{x}{c}\right| - \frac{1}{2}\left(1-\frac{x}{c}\right)^2 \\ log_e\left|1-\frac{x}{c}\right| + \frac{1}{4}\left(1-\frac{x}{c}\right)^2 - \frac{1}{4}\left(a-\frac{x}{c}\right)^2 \end{matrix}\right] \\ -\frac{x}{c} log_e\left(\frac{x}{c}\right) + g - h\frac{x}{c} \end{matrix}\right\}} \\ g = \frac{1}{1-a}\left[a^2\left(\frac{1}{2} log_e\, a - \frac{1}{4}\right) + \frac{1}{4}\right] \\ h = \frac{1}{1-a}\left[\frac{1}{2}(1-a)^2 log_e(1-a) - \frac{1}{4}(1-a)^2\right] + g \\ C_{li_{mod}} = \frac{C_{li}}{1.0209} \quad for\ 0 \prec \left[\frac{x}{c} = a = 0.831\right] \prec 0.87437 \end{cases} \quad (5)$$

Hence, for our chosen airfoil NACA 64A204, we have the following expression

$$y_c^{F16}(x) = \begin{bmatrix} 3.479\, ln(|-0.831 + 0.01x|) - 0.084\, ln(|-0.831 + 0.01x|)\, x \\ +5.038 * 10^{-4}\, ln(|-0.831 + 0.01x|)\, x^2 - 5.038 * 10^{-4}\, ln(|-1 + 0.01x|)\, x^2 \\ +1.007 * 10^{-1}\, ln(|-1 + 0.01x|)\, x - 5.038\, n(|-1 + 0.01x|) + 0.644 + 0.107x \\ -1.703 * 10^{-2} x\, ln(x) \end{bmatrix} \quad (6)$$

As for thickness distributions, there is no exact analytical definition for 6-series NACA airfoils, mostly done through a result of numerical methods which produced tabulated coordinates. However, the closest approximation for an analytical expression for thickness distribution (characterizing the half-thickness of the airfoil for x) is the following [17]:

$$\frac{y_t}{c} = \frac{t}{0.2}\left[0.2969\sqrt{\frac{x}{c}} - 0.126\frac{x}{c} - 0.3516\left(\frac{x}{c}\right)^2 + 0.2843\left(\frac{x}{c}\right)^3 - 0.1036\left(\frac{x}{c}\right)^4\right] \quad (7)$$

Similarly, NACA 64A204 the expression of thickness distribution is

$$y_t^{F16}(x) = \begin{bmatrix} 593.8\sqrt{x} - 20.72 * 10^{-6}x^4 + 5.69 * 10^{-3}x^3 \\ -703.2 * 10^{-3}x^2 - 25.2x \end{bmatrix} \quad (8)$$

Nevertheless, for the rest of the calculations, since the profile is supposed to be thin, it is necessary to show the relative thickness in the equations of the extrados, in the form [18]:

$$y = \varepsilon h(x) \quad (9)$$

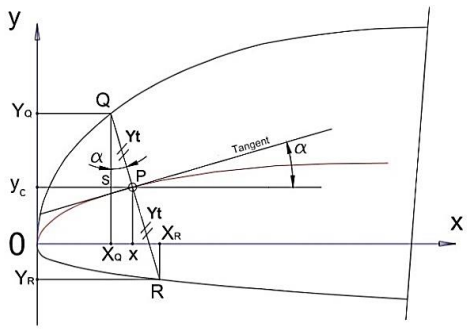

Fig. 17. Coordinate Projection

Following the projection (See Fig.17.), the formula used to determine the value of the height of the extrados for a selected point $Q(x_Q, y_Q)$ is of the following form:

$$\begin{cases} x_Q = x - y_t\, sin(\alpha) \\ y_Q = y_c + y_t\, cos(\alpha) \end{cases} \text{ with } \alpha = arctan\left(\frac{dy_c}{dx}\right) \quad (10)$$

With $y_Q = \varepsilon h_Q(x)$ for

$$h_Q(x) = \frac{1}{\varepsilon}[y_c(x) + y_t(x)\, cos(\alpha)] \quad (11)$$

Finally, with these extrados Thickness equations, the NACA 64A204 airfoil can be accurately modelled. Interestingly, these formulas are actually valid for any thin airfoil. Hence, after calculations we got the equation of the extrados curve in $y(x)$ as following:

$$\begin{cases} y_1(x) \cong 1.4574x - 148.4546x^2 \\ \rightarrow For\ 0.002219 \leq x \prec 0.0039426 \\ y_2(x) \cong \dfrac{\begin{bmatrix} 7.8283*10^{-13} + 1.0178*10^{-1}x^8 - 2.3723*10^{-2}x^7 \\ -5.0395*10^{-4}x^6 + 4.1529*10^{-4}x^5 \\ -3.5898*10^{-5}x^4 + 1.293*10^{-6}x^3 - \\ 2.0646*10^{-8}x^2 + 9.1687*10^{-11}x \end{bmatrix}}{\begin{bmatrix} 3.934*10^{-10} + x^7 - 3.5901*10^{-1}x^6 + 4.1242*10^{-2}x^5 \\ -1.8993*10^{-3}x^4 + 1.6406*10^{-5}x^3 \\ +1.33312*10^{-6}x^2 - 4.175*10^{-8}x \end{bmatrix}} \\ \rightarrow For\ 0.0061558 \leq x \prec 0.1049225 \\ y_3(x) \cong 8.3094 * 10^{-3} + 1.2213 * 10^{-1}x - 1.6721 * 10^{-1}x^2 + 3.6633 * 10^{-2}x^3 \\ \rightarrow For\ 0.1049225 \leq x \leq 1 \end{cases} \quad (12)$$

Now we can calculate Analytical Local Mach numbers at 30%c and 60%c for NACA64A204 based on our previously established analytical model [1]-[2].

5.1.2 Analytical Local Mach Number for NACA64A204

For F-16 airfoil NACA 64A204, at 30%c and 60%c Pressure Taps, we get the following analytical results (See Table III):

Table 3 Analytical Local Mach Number Values in The Pressure Taps for NACA 64A204 after Calculations

Mach Upstream	Pressure Tap	Local Analytical Mach Number
1.55	Pressure Tap N^{26}	1.413532608
1.55	Pressure Tap N^{27}	1.516532226
1.44	Pressure Tap N^{26}	1.332598661
1.44	Pressure Tap N^{27}	1.466334279

5.2 Results Comparison

In this part, we are interested in comparing the Local experimental, analytical and numerical Mach number values at 30%c and 60%c, additionally, we will be comparing the angles of the detached curved SW and its distance from the leading edge both numerically and experimentally.

The purpose of this comparison is to find to which extent our analytical model [1]-[2] is valid for the case of a supersonic laminar thin airfoil, as well as to validate our designed F-16 airfoil mock-ups.

5.2.1 Local Mach Number Comparison

After comparing numerical-analytical-experimental values for Local Mach number at 30%c for NACA 64A204 we can find that the results are very similar, with relative errors below $\varepsilon_{30\%c} = 2\%$.

However, at 60%c when approaching the trailing edge, we can see that the relative errors slightly increase while always maintaining a relative error below $\varepsilon_{60\%c} = 6\%$. (See Table 4 for data).

Table 4 Numerical-Experimental-Analytical Local Mach Number at 30%c & 60%c for NACA 64A204 with Relative Errors for Values

Mach Upstream	Pressure Tap	Local Analytical Mach Number	Local Numerical Mach Number	Local Experimental Mach Number	Relative Error in %	
1.55	Pressure Tap N[26]	1.413532608	1.42307	1.42	1.18968	**Num-Exp**
					1.87243	**Num-Analytical**
1.55	Pressure Tap N[27]	1.516532226	1.5296	1.47	3.89644	**Num-Exp**
					3.06833	**Num-Analytical**
1.44	Pressure Tap N[26]	1.332598661	1.3219	1.33	1.36924	**Num-Exp**
					0.55541	**Num-Analytical**
1.44	Pressure Tap N[27]	1.466334279	1.4257	1.38	3.20544	**Num-Exp**
					5.88776	**Num-Analytical**

5.2.2 Comparison of Angles of Detached Curved SW and Its Distance from The Leading Edge

Taking into consideration the angles of the detached curved SW from experimentation in SBWT AF300 and numerical simulations in Ansys Fluent 2022 R2, the errors between the values βext and σext, also between β_{int} and σ_{int} for an M_0*=1.44* are as follows:

$$\varepsilon_{ext} = 12.72\% \ and \ \varepsilon_{int} = 11.11\%$$

As for the distance between the Detached SW and the leading edge of the NACA 64A204 airfoil, the analytical-numerical-experimental values for M_0*=1.44* are as follows (See Table 5):

Table 5 Numerical-Experimental-Analytical Distance between Detached SW and Leading edge for NACA 64A204

Mach Upstream	Distance for Experiment	Distance for Simulation	Distance analytically *
M_0	Δ_{exp}	Δ_{num}	Δ_{anly}
1.44	3,48 cm	2.687 cm	4.51416 cm

**See Appendix for calculation of analytical distance between detached SW and the leading edge of the airfoil*

Thus, it is possible to determine the relative errors of the analytical distance Δ_{anly} then numerical Δ_{num} for M_0=1.44 with this experimental value:

$$\varepsilon^{\Delta}_{num} = 22.787\% \text{ and } \varepsilon^{\Delta}_{analy} = 29.7172\%$$

These deviations seem large when the distances are compared to each other, but compared to the overall size of the airfoil, therefore to the chord, they are negligible. They correspond to a difference of half a centimetre. It is assumed that the viscosity of the air which cannot be neglected in the wind tunnel is the cause.

6. Discussion & Conclusion

In this study, we managed to prove the validity of our designed 3D-printed and manually manufactured F-16 NACA64A204 airfoil mock-ups. The mock-ups were the subject of experimentation in the SBWT AF300 for a chosen tunnel section of M0=1.4.

The numerical simulation in Ansys Fluent 2022 R2 and the theoretical approach [1]-[2] has helped not only to describe numerically the different phenomena governing SWBLI around the thin airfoil but also to confirm the validity and effectiveness of the technics adopted for our mock-up, first for our 3D-printed mock-up by comparing the angles of the detached curved SW and its distance from the leading edge of the airfoil numerically, experimentally and analytically, the relative errors between values were of average approx. 26% for the angles and 12% for the distance, the reason for these errors being moderately high is due to the 3D-printed mock-up was too fragile and not resisting vibrations and supersonic gusts, and the visualization of the shock waves was approximate in the SBWT.

Nevertheless, the precision of the theoretical and numerical models slightly catches up with the experimental hazards, since the data of the angles measured are not reliable but remain consistent to the order of magnitude.

Additionally, for the comparison of the local Mach number at 30%c and 60%c for NACA 64A204, with our manually manufactured mock-up, firstly for the 1st Pressure Tap, the error between the analytical-numerical-experimental results was negligible at an average below 2%, which greatly validates, at a first instance, our designed model and improved theoretical model. As for the 2nd Pressure Tap, the average error between the analytical-numerical-experimental results increases slightly but always stays under 6%, which also validates greatly of mock-up and analytical model. The reason for which the errors are all under 6% is thanks to the airfoil we opted for in our study which is a laminar airfoil, helping to maintain a laminar flow up to 80%c and then a quasi-transitional flow until the trailing edge due to the benefit of the eliminated cusp in NACA 6A-series airfoils.

However, the slight increase can be given to the fact that the flow at the exit of the nozzle of the wind tunnel which could be not perfectly horizontal because of the shape of the profile of the nozzle, so the flow will take a form similar to the shape of the profile. This could therefore result in a streamline that is not perfectly horizontal at the level of the experimental wing airfoil, which would influence the incidence of the fluid upstream and therefore the acquisitions of pressure tapping.

Finally, this study not only allowed us to validate our designed mock-ups, allowing us to open the door for several other airfoils to be tested and ensure maximum exploitation of SBWT AF300 in the field of scientific research, additionally we managed to prove once again the validity of our previously established theoretical model at a high percentage of the chord thanks to the choice of a laminar supersonic airfoil, and last but not least, we were able to study and dissect different phenomena that govern viscous supersonic flows around NACA 6A-Series airfoil.

APPENDIX

In theory, the distance Δ_{analy} between the curved shock wave and the leading edge is found using the following formula:

$$\Delta_{anly} = R \times 0.386 e^{\frac{4.67}{M_0^2}}$$

Where R is the radius of the leading edge of NACA 64A204, for a chord equal to one meter it equals: R=1.23 cm.

ACKNOWLEDGEMENTS

The authors would like to express profound gratitude and respect to the late Professor Mohammed HASNAOUI, who passed away due to Covid 19 during this study, in December 2020. His outstanding morality, astonishing expertise in the field of fluid mechanics and asymptotical modelling, as well as supervising role were very enriching; we, as a team, are honoured to have been his pupils.

REFERENCES

El-Aajine, O., N. Eddegdag, A. Naamane, M. Radouani, and B. El Fahime. "Asymptotic Modeling of a Viscous Laminar Flow Around Thin Airfoils: Resolution and Experimental Treatment in Case of Supersonic Flow." *International Review of Mechanical Engineering (I.RE.M.E.)*, Vol. 16, n. 1 (2022).

N. Eddegdag, El-Aajine, O., A. Naamane and M. Radouani. " Improved Analytical/Statistical Modelling of the Shock Wave-Laminar Boundary Layer Around a Thin Airfoil: Standard Atmosphere Case" To be published in *Advances in Integrated Design & Production II- International Conference on Integrated Design and Production Proceedings 2022*, pp. xxx-xxx. Springer, 2023.
Arxiv URL:
https://arxiv.org/submit/4661338/view

Li, B., Zhou, D. L., Wang, Y., Shuai, Y., Liu, Q. Z., & Cai, W. H. The design of a small lab-scale wind turbine model with high performance similarity to its utility-scale prototype. *Renewable Energy*, 149, 435-444. (2020).

He, Shun, Shijun Guo, Ying Liu, and Wukui Luo. "Passive gust alleviation of a flying-wing aircraft by analysis and wind-tunnel test of a scaled model in dynamic similarity." *Aerospace Science and Technology* 113 (2021): 106689.

Ladson, Charles L., Cuyler W. Brooks Jr, Acquilla S. Hill, and Darrell W. Sproles. *Computer program to obtain ordinates for NACA airfoils*. No. L-17509. 1996.

Abbott, Ira H., Albert E. von Doenhoff, and Louis Stivers Jr. *Summary of airfoil data*. No. NACA-TR-824. 1945.

Patterson, Elizabeth W., and Albert L. Braslow. *Ordinates and Theoretical Pressure-distribution Data for NACA 6-and 6A-series Airfoil Sections with Thicknesses from 2 to 21 and from 2 to 15 Percent Chord, respectively*. National Aeronautics and Space Administration, 1961.

TecQuipment. *AF300 Supersonic Burst Wind Tunnel User Manual*. (2011).

Ives, Rob, Edet BASSEY, and Faik A. HAMAD. "Investigation of the flow around an aircraft wing of section NACA 2412 utilising ANSYS fluent." *INCAS Bulletin 10*, no. 1 (2018).

Naamane, A., and M. Hasnaoui. "Supersonic Flow around a Dihedral Airfoil: Modeling and

Experimentation Investigation." *International Journal of Aerospace and Mechanical Engineering* 13, no. 6 (2019): 413-417.

M.Hasnaoui, A. Naamane, H. Akhmari, Asymptotic modeling the

aerodynamic coefficients of the NACA Airfoil. Modeling, *IIETA Journals, Measurement and Control B* Vol. 88, No. 2-4, Page: 58-66 (2019)

Billig, Frederick S. "Shock-wave shapes around spherical-and cylindrical-nosed bodies." *Journal of Spacecraft and Rockets* 4, no. 6 (1967): 822-823.

Zeytounian, Radyadour Kh. "*Singular Coupling and the Triple-Deck Model*." Asymptotic Modelling of Fluid Flow Phenomena (2002): 471-525.

Abbott IH, Von Doenhoff AE. *Theory of wing sections: including a summary of airfoil data*. Courier Corporation; 2012 Apr 26.

Loftin Jr, Laurence K. *Theoretical and experimental data for a number of NACA 6A-series airfoil sections*. No. NACA-RM-L6J01. 1946.

Jacobs, Eastman N. Preliminary report on laminar-flow airfoils and new methods adopted for airfoil and boundary-layer investigations. *National Aeronautics and Space Admin Langley Research Center Hampton* VA, 1949

Jacobs, Eastman Nixon, Kenneth Edwards Ward, and Robert McLean Pinkerton. The Characteristics of 78 related airfoil section from tests in the Variable-Density Wind Tunnel. No. 460. *US Government Printing Office*, 1933.

Series, NACA Four-Digit. "*The NACA airfoil series."* (2012).

James Campbell & Rade Vignjevic. *Artificial Viscosity Methods for Modeling Shock Wave Propagation* (June 2009).

Doi: 10.1007/978-1-4419-0727-1_19

José Pontes, Norberto Mangiavacchi, Gustavo Rabello dos Anjos, *An Introduction to Compressible Flows with Applications Quasi One Dimensional Approximation and General Formulation for Subsonic, Transonic, and Supersonic Flows* p. 43 (Springer International Publishing, 2019).

Boin, J-Ph, J. Ch Robinet, Ch Corre, and H. Deniau. "3d steady and unsteady bifurcations in a shock-wave/laminar boundary layer interaction: a numerical study." *Theoretical and Computational Fluid Dynamics* 20, no. 3 (2006): 163-180.

Winslow, Justin, Hikaru Otsuka, Bharath Govindarajan, and Inderjit Chopra. "Basic understanding of airfoil characteristics at low Reynolds numbers (10 4–10 5)." *Journal of Aircraft* 55, no. 3 (2018): 1050-1061.